1   **Title**: Decomposing leaf mass into photosynthetic and structural components explains
2   divergent patterns of trait variation within and among plant species
3
4   **Running title**: Photosynthetic and structural leaf mass
5

6   **Authors**: Masatoshi Katabuchi[1,2], Kaoru Kitajima[1,3,4], S. Joseph Wright[4], Sunshine A. Van
7   Bael[4,5], Jeanne L. D. Osnas[1] and Jeremy W. Lichstein[1]
8
9   [1] Department of Biology, University of Florida, Gainesville, FL 32611, USA
10   [2] Department of Agricultural and Biological Engineering, University of Florida, Gainesville,
11   FL 32611, USA
12   [3] Graduate School of Agriculture, Kyoto University, Kitashirakawa Oiwake-Cho, Kyoto 606-
13   8502 Japan
14   [4] Smithsonian Tropical Research Institute, 9100 Panama City Pl., Washington, DC 20521
15   [5] Department of Ecology and Evolutionary Biology, Tulane University, New Orleans, LA
16   70118 USA
17

18   **Total word count:** 5915
19   **Summary:** 200
20   **Introduction:** 1245
21   **Material and Methods:** 2190
22   **Results:** 981
23   **Discussion:** 1427
24   **Acknowledgments:** 72
25   **Number of figures:** 6
26   **Number of tables:** 0
27   **Number of SI files:** 1 (Notes S1-4, Fig. S1-5, and Table S1-4)
28

29   **Author for correspondence:** Masatoshi Katabuchi
30   **Mailing address:** Department of Biology, University of Florida, Gainesville, FL 32611,
31   USA
32   **Email:** mattocci27@gmail.com
33   **Telephone**: 352-392-1540
34
35

Abstract

- Across the global flora, photosynthetic and metabolic rates depend more strongly on leaf area than leaf mass. In contrast, intraspecific variation in these rates is strongly mass-dependent. These contrasting patterns suggest that the causes of variation in leaf mass per area (LMA) may be fundamentally different within vs. among species.

- We used statistical methods to decompose LMA into two conceptual components – 'photosynthetic' LMAp (which determines photosynthetic capacity and metabolic rates, and also affects optimal leaf lifespan) and 'structural' LMAs (which determines leaf toughness and potential leaf lifespan) using leaf trait data from tropical forest sites in Panama and a global leaf-trait database.

- Statistically decomposing LMA into LMAp and LMAs provides improved predictions of trait variation (photosynthesis, respiration, and lifespan) across the global flora, and within and among tropical plant species in Panama. Our analysis shows that most interspecific LMA variation is due to LMAs (which explains why photosynthetic and metabolic traits are area-dependent across species) and that intraspecific LMA variation is due to changes in both LMAp and LMAs (which explains why photosynthetic and metabolic traits are mass-dependent within species).

- Our results suggest that leaf trait variation is multi-dimensional and is not well-represented by the one-dimensional leaf economics spectrum.

Keywords: Bayesian inference, functional diversity, global vegetation models, interspecific variation, intraspecific variability, latent variables, null models, optimal leaf lifespan

Introduction

Over the past two decades, the 'leaf economics spectrum' (LES) (Reich *et al.*, 1997; Wright *et al.*, 2004; Reich, 2014) has become a cornerstone of plant ecology. The LES captures tight relationships among leaf mass per area (LMA), leaf lifespan (LL), and mass-normalized leaf traits related to carbon fixation and nutrient use, suggesting the presence of a single dominant axis of leaf functional variation, ranging from short-lived leaves with high photosynthetic potential and fast returns on investment to long-lived leaves with low photosynthetic potential and slow returns (Wright *et al.*, 2004; Westoby & Wright, 2006; Reich, 2014). Because the mass-based LES constrains variation in green leaf traits to a single axis, it has been proposed as a simple framework for incorporating more realistic levels of

69   leaf trait diversity in global carbon-climate models (Bonan *et al.*, 2002; Wright *et al.*, 2004).

70   However, recent analyses suggest that the one-dimensional LES is largely the result of high

71   interspecific variation in LMA combined with mass-normalization of area-dependent traits

72   (Osnas *et al.*, 2013; Lloyd *et al.*, 2013).

73   The essence of the problem follows (see Osnas *et al.* 2013 and Notes S1 for details).

74   Let X represent the whole-leaf value of a purely area-dependent trait; i.e., X is proportional to

75   leaf area, where X could be the photosynthetic capacity of the entire leaf (units = moles CO_2

76   fixed per-unit time), the amount of nitrogen in the entire leaf (units = grams of nitrogen), etc.

77   The mass-normalized trait value would then be X/Mass, which (assuming X is proportional to

78   leaf area) is proportional to Area/Mass = LMA^{-1}. This simplistic example shows that if traits

79   are actually area-dependent, mass normalization can introduce spurious correlations; i.e., in

80   this example, X/Mass is proportional to LMA^{-1}, even though X is assumed to depend only on

81   leaf area. Thus, the strong correlations observed among LMA and mass-normalized traits

82   (Reich et al. 1997; Wright et al. 2004) should not be taken as evidence for a single dominant

83   axis of leaf functional variation (Osnas *et al.*, 2013; Lloyd *et al.*, 2013).

84   An important observation suggesting the presence of multiple axes of leaf functional

85   variation is that trait relationships across species are sometimes inconsistent with those

86   observed within species. For example, across species in the global flora, LMA has a strong,

87   positive relationship with LL but a weak relationship with net photosynthetic capacity per-

88   unit leaf area (A_{area}) (Wright *et al.*, 2004). In contrast, intraspecific variation in these traits

89   across vertical canopy (light) gradients shows the opposite pattern: within species, LMA has

90   a weak and/or negative relationship with LL (Osada *et al.*, 2001; Lusk *et al.*, 2008; Russo &

91   Kitajima, 2016) but a strong, positive relationship with A_{area} (Ellsworth & Reich, 1993;

92   Kenzo *et al.*, 2006; Niinemets *et al.*, 2014). These contrasting patterns suggest that the causes

93   of LMA variation may be fundamentally different within vs. among species. Furthermore,

94   variation in four traits related to photosynthesis and metabolism – net photosynthetic

95   capacity, dark respiration rate, and concentrations of nitrogen and phosphorus – are primarily

96   mass-dependent among species within some plant functional groups, and primarily area-

97   dependent within others (Osnas *et al.*, in review). Thus, leaf trait relationships diverge in a

98   number of intra- and interspecific comparisons, suggesting the presence of multiple axes of

99   functional variation that can combine in different ways to create a variety of patterns.

100   A conceptual model that might explain these divergent patterns is to view LMA as

101   being comprised of two primary components – 'photosynthetic' leaf mass (LMAp, which

102   determines photosynthetic capacity and associated metabolic activity, such as phloem-

3

103   loading) and structural leaf mass (LMAs, which determines toughness and thus potential LL)

104   (Osnas *et al*., in review). This conceptual model can potentially explain the above divergent

105   trait patterns, because variation in LMAp leads to mass-dependence of photosynthetic and

106   metabolic traits, whereas variation in LMAs leads to area-dependence of these same traits

107   (Notes S2). Thus, the degree of area- vs. mass-dependence in a given leaf assemblage should,

108   according to this conceptual model, depend on the relative contributions of LMAp and LMAs

109   to total LMA variation in the assemblage.

110   A challenge to implementing the above conceptual model is the absence of direct

111   measurements of LMAp and LMAs. Although some leaf mass components are clearly

112   associated with certain functions (e.g., chloroplasts perform photosynthesis), it is difficult to

113   neatly partition some leaf mass components to specific functions. For example, thick cell

114   walls provide structural toughness and allow for long LL (Kitajima *et al.*, 2012), but a leaf

115   without any cell wall mass would lack the biomechanical support needed to intercept light

116   and perform photosynthesis. Thus, it is difficult to determine how much of the cell wall mass

117   present in a leaf was constructed for photosynthesis and associated metabolic functions, vs.

118   how much additional cell wall mass was constructed for the purpose of prolonging LL.

119   Despite this challenge, it should be possible to use multivariate trait datasets to statistically

120   partition LMA into LMAp and LMAs, because statistical relationships among net

121   photosynthetic capacity (A_{max}), dark respiration rate (R_{dark}), LMA, and LL should hold clues

122   regarding the allocation of leaf mass to photosynthetic vs. structural functions.

123   In this paper, we explore the above conceptual model using leaf trait data from two

124   tropical forest sites (sun and shade leaves from wet and dry sites in Panama) and the

125   GLOPNET global leaf traits database (Wright *et al.* 2004). For simplicity, our analysis

126   assume that LMA is equal to the sum of separate additive components, LMAp and LMAs.

127   The goal of our analysis is to evaluate if the conceptual model described above can explain

128   divergent patterns in leaf trait data, and if so, to use the model to elucidate the causes of these

129   divergent patterns. First, we describe a statistical modeling framework to estimate LMAp and

130   LMAs, and we use simulations to show that the model yields robust results that are not prone

131   to statistical artifacts. Then, we ask the following questions: (1) Does decomposing LMA into

132   photosynthetic and structural components lead to improved predictions of A_{max}, R_{dark}, and

133   LL? (2) What is the relative importance of LMAp vs. LMAs in explaining variation in LMA

134   within and among species? (3) Do LMAp and LMAs differ between evergreen and deciduous

135   species, and between sun and shade leaves? and (4) How are measurable leaf photosynthetic

136   and structural traits (e.g., concentrations of nitrogen and cellulose) related to LMAp and

137   LMAs?

138   Our model is conceptually similar to that of Shipley *et al.* (2006), which explained the

139   LES in terms of a tradeoff between the volume of a leaf allocated to cell wall vs. protoplasm.

140   An important difference between our analysis and that of Shipley *et al.* (2006) is that our goal

141   is to understand divergent trait patterns within vs. among species, whereas Shipley *et al.*

142   (2006) focused only on interspecific variation. Because we treat LMA as the sum of LMAp

143   and LMAs without considering how these mass components are packaged within a leaf, our

144   model ignores the effects of leaf anatomy. For example, a given cell wall mass per leaf area

145   may be packaged into a large surface area with thin walls (high mesophyll conductance and

146   A_{max}, but low structural toughness) or a small surface area with thick walls (low mesophyll

147   conductance and A_{max}, but high structural toughness) (Onoda *et al.*, 2017). Despite its lack of

148   anatomical detail, our model explains much of the inter- and intraspecific variation in A_{max},

149   R_{dark}, and LL (see Results) and provides novel insights into the causes of divergent patterns of

150   trait variation within vs. among species (see Discussion).

151

152   **Material and Methods**

153   **Model overview**

154   We developed a statistical modeling framework to partition LMA into additive LMAs and

155   LMAp components (see below and Notes S3). For sample i (where 'sample' refers to a

156   species, or a species $\times$ canopy position combination; see Datasets below), we partition LMA_i

157   into $LMAp_i = f_i \times LMA_i$ and $LMAs_i = (1 - f_i) \times LMA_i$ by estimating a latent variable f_i. The

158   latent variables f_i are not directly observed, but they can be constrained by available data

159   using Bayesian methods (Bishop, 2006; Gelman & Hill, 2006). For example, posterior

160   distributions for $LMAp_i$ should tend to converge on high values for leaves with high A_{area},

161   and posterior distributions for $LMAs_i$ should tend to converge on high values for leaves with

162   high LL. Given the large number of free parameters (i.e., one latent variable per leaf sample),

163   it is possible for the model to over-fit the data, which could lead to spurious inferences.

164   Therefore, we performed tests with randomized data (see below) and with simulated data to

165   evaluate model performance under a range of conditions (Notes S4). Tests with simulated

166   data suggest that our modeling approach is robust and not prone to producing artefactual

167   results.

168

5

169 **Modeling leaf lifespan, photosynthetic capacity, and dark respiration in relation to**

170 **photosynthetic and structural leaf mass components**

171 We assume that the sum of photosynthetic leaf mass per area (LMAp) and structural leaf

172 mass per area (LMAs) is equal to total observed LMA for leaf sample i (where a 'sample' is a

173 species in the GLOPNET dataset, or a species $\times$ canopy position combination in the Panama

174 dataset):

175 $\quad \mathrm{LMA}_i = \mathrm{LMAp}_i + \mathrm{LMAs}_i$ (1)

176 $\quad \mathrm{LMAp}_i = f_i \mathrm{LMA}_i$ (2)

177 $\quad \mathrm{LMAs}_i = (1 - f_i) \mathrm{LMA}_i$ (3)

178 where, f_i is the fraction of LMA_i that is comprised of LMAp_i. The f_i terms are not directly

179 observed but can be estimated as latent variables in a Bayesian modeling framework (see

180 details below). In our model, gross photosynthetic capacity (approximated here as the sum of

181 A_{area} and R_{area}) is determined by LMAp, LL is determined by LMAs, and total leaf dark

182 respiration is the sum of respiration components due to photosynthetic and structural tissues:

183 $\quad \mathrm{E[gross\ photosynthesis]} = \mathrm{E}[A_{\mathrm{area}\,i} + R_{\mathrm{area}\,i}] = \alpha \mathrm{LMAp}_i = \alpha f_i \mathrm{LMA}_i$ (4)

184 $\quad \mathrm{E[LL}_i] = \beta_1 \mathrm{LMAs}_i = \beta_1 (1 - f_i) \mathrm{LMA}_i$ (5, Potential LL Model)

185 $\quad \mathrm{E}[R_{\mathrm{area}\,i}] = r_p \mathrm{LMAp}_i + r_s \mathrm{LMAs}_i = r_p f_i \mathrm{LMA}_i + r_s (1 - f_i)\,\mathrm{LMA}_i$ (6)

186 where, $\mathrm{E}[\cdot]$ is the expected value of the variable in brackets, $A_{\mathrm{area}\,i}$, $R_{\mathrm{area}\,i}$, and LL_i, are,

187 respectively, the net photosynthetic rate ($A_{\max}$) per unit area, dark respiration rate (R_{dark}) per

188 unit area, and leaf life span of leaf i; α is net photosynthetic rate per unit photosynthetic

189 mass; β_1 is leaf lifespan per unit structural mass; and r_p and r_s, are, respiration rates per unit

190 photosynthetic and structural leaf mass, respectively. Eq. 5 is labeled "Potential LL Model",

191 because this model assumes that LL is affected only by structural toughness (which we

192 assume is proportional to LMAs), in contrast to an alternative model based on optimal LL

193 theory (see Eqs. 12-14 below). The logarithms of gross photosynthesis, LL, and R_{area} are

194 assumed to have a multivariate normal distribution (MVN):

195 $\quad \begin{pmatrix} \ln\,[A_{\mathrm{area}\,i} + R_{\mathrm{area}\,i}] \\ \ln\,[\mathrm{LL}_i] \\ \ln\,[R_{\mathrm{area}\,i}] \end{pmatrix} \sim \mathrm{MVN} \begin{pmatrix} \mu_{1i} \\ \mu_{2i}, \boldsymbol{\Sigma} \\ \mu_{3i} \end{pmatrix}$ (7)

196 $\quad \mu_{1i} = \ln \alpha + \ln f_i + \ln \mathrm{LMA}_i - \frac{\sigma_1^2}{2}$ (8)

197 $\quad \mu_{2i} = \ln \beta_1 + \ln(1 - f_i) + \ln \mathrm{LMA}_i - \frac{\sigma_2^2}{2}$ (9)

198 $\quad \mu_{3i} = \ln[r_p f_i \mathrm{LMA}_i + r_s(1 - f_i)\mathrm{LMA}_i] - \frac{\sigma_3^2}{2}$ (10)

6

199 $$\Sigma = \begin{pmatrix} \sigma_1^2 & \rho_{12}\sigma_1\sigma_2 & \rho_{13}\sigma_1\sigma_3 \\ \rho_{12}\sigma_1\sigma_2 & \sigma_2^2 & \rho_{23}\sigma_2\sigma_3 \\ \rho_{13}\sigma_1\sigma_3 & \rho_{23}\sigma_2\sigma_3 & \sigma_3^2 \end{pmatrix}$$ (11)

200 where μ_{1-3} are, respectively, the expected values of $\ln[A_{\text{area } i} + R_{\text{area } i}]$, $\ln[LL_i]$, and $\ln[R_{\text{area } i}]$

201 (from Eqs. 4-6); Σ is the covariance matrix; σ_1, σ_2, and σ_3 are standard deviations of μ_{1-3}; and

202 ρ_{12}, ρ_{13}, and ρ_{23} are correlation coefficients among μ_{1-3} (e.g., we expect positive covariance

203 between μ_1 and μ_3 because both include $R_{\text{area } i}$).

204   In addition to Eq. 5 (Potential LL Model), we considered an alternative assumption

205 for the relationship between LL and other traits based on optimal LL theory (Kikuzawa,

206 1991; Kikuzawa *et al.*, 2004; 2013). According to this theory, the optimal leaf lifespan

207 (LL_{opt}) maximizes a leaf's lifetime carbon gain per-unit time, which is determined by

208 potential LL, net photosynthetic rate, and construction cost per unit leaf area:

209 $$LL_{\text{opt}} = \sqrt{2bC/(a-m)}$$ (12)

210 where a is the realized (i.e., light-dependent) gross photosynthetic rate per unit leaf area, m is

211 the realized daily respiration rate per unit leaf area, b is the rate of decline in photosynthetic

212 capacity with leaf age (which determines potential LL in the Kikuzawa model), and C is the

213 construction cost per unit leaf area. To implement this Optimal LL Model, we assumed that

214 (i) potential LL is proportional to LMAs; and (ii) leaf construction cost per unit area (g

215 glucose per unit leaf area) is proportional to LMA. Assumption (ii) is justified because leaf

216 construction cost per unit mass (g glucose per unit leaf mass) is strongly conserved (Williams

217 *et al.*, 1989; Villar & Merino, 2001). Thus, Eq. 12 can be written in terms of the traits

218 considered in our analysis as:

219 $$\begin{aligned} E[LL_i] &= \beta_2\sqrt{LMAs_i LMA_i/(\theta_L A_{\text{area } i} - R_{\text{area } i})} \\ &= \beta_2\sqrt{(1-f_i)LMA_i^2/(\theta_L A_{\text{area } i} - R_{\text{area } i})} \end{aligned}$$ (13, Optimal LL Model)

220 where β_2 is a constant, and θ_L ($0 < \theta_L < 1$) is a scaling parameter that accounts for the effects

221 of light availability on the realized photosynthetic rate (Kikuzawa *et al.*, 2004) (see Notes

222 S3). The expected value of the logarithm of LL (μ_{2i} in Eq. 7) for the Optimal LL Model is:

223 $$\mu'_{2i} = \ln\beta_2 + \ln LMA_i + \frac{1}{2}[\ln(1-f_i) - \ln(\theta_L A_{\text{area } i} - R_{\text{area } i})] - \frac{\sigma'^2_2}{2}.$$ (14)

224   We fit the Optimal LL Model to the Panama data (see Methods/Datasets in main text),

225 which includes both sun and shade leaves for 26 out of 106 total species. We set $\theta_L = 1$ for

226 sun leaves, and we fit θ_L as a single free parameter assigned to all shade leaves. We

227 considered versions of the Optimal LL Model both with and without an additional parameter

228   to account for differences in LL between the dry and wet sites due to mechanisms not

229   included in the model (Notes S3).

230

Datasets

232   To fit the models described above, we used LMA (g m^{-2}), net photosynthetic capacity per unit

233   leaf area (A_{area}; μmol s^{-1} m^{-2}), dark respiration rate per unit leaf area (R_{area}; μmol s^{-1} m^{-2}) and

234   LL (months) from the GLOPNET global leaf traits database (Wright *et al.*, 2004) and from

235   two tropical forest sites in Pana

236   ma: Monumental Natural Metropolitano (MNM, "dry site") and Bosque Protector San

237   Lorenzo (SL, "wet site"). The Panama data include leaves sampled at two canopy positions

238   ("sun": full sun at the top of the canopy; and "shade": well shaded, sampled within 2 m of the

239   forest floor) from trees within reach of a canopy crane at each site. The dry MNM site is a

240   semi-deciduous coastal Pacific forest with a 5-month dry season from December-April and

241   1740 mm of annual rainfall (Wright *et al.*, 2003). The MNM crane is 40 m tall with a 51 m

242   long boom. The wet SL site is an evergreen Caribbean coastal forest with 3100 mm of annual

243   rainfall (Wright *et al.* 2003). The SL crane is 52 m tall with a 54 m long boom.

244   After deleting leaf samples (i.e., database records, which typically average over

245   multiple individual leaves) that lacked one of the four traits (LMA, A_{area}, R_{area}, or LL), 198

246   samples for 198 unique species were available for GLOPNET, and 132 samples for 106

247   unique species were available for Panama (dry and wet sites combined; 26 species sampled in

248   both sun and shade; no species with all four traits available at both sites). Both datasets

249   include additional traits that we used to interpret model results, but which were not used to fit

250   models. These traits include nitrogen and phosphorus content per leaf unit area (N_{area} and

251   P_{area}; g m^{-2}) in both datasets, leaf habit in GLOPNET (deciduous or evergreen), and cellulose

252   content per unit area (CL_{area}; g m^{-2}) in Panama.

253   We fit the Potential LL Model (Eq. 5) to both GLOPNET and Panama data. We fit the

254   Optimal LL Model (Eq. 13; Notes S3) only to the Panama data because GLOPNET primarily

255   represents interspecific variation among sun leaves, whereas the Optimal LL Model was

256   motivated by the negative intraspecific LL-LMA relationship observed in Panama (Osnas *et*

257   *al*. *in review*) and elsewhere (Lusk *et al.*, 2008).

258

Parameter estimation

8

260   We used independent and non-informative prior distributions for all parameters, including

261   latent variables f_i for each leaf sample. All priors were non-informative. The covariance

262   matrix in Eq.11 in main text was decomposed as $\mathbf{\Sigma} = \text{diag}(\mathbf{\sigma})\,\mathbf{\Omega}\,\text{diag}(\mathbf{\sigma}) = \text{diag}(\mathbf{\sigma})\,\mathbf{LL'}$

263    $\text{diag}(\mathbf{\sigma})$ using a Cholesky decomposition, where $\mathbf{\sigma}$ is a vector of σ_1, σ_2 and σ_3; $\mathbf{\Omega}$ is a

264   correlation matrix of ρ_{12}, ρ_{13}, and ρ_{23}; and $\mathbf{L}$ is a lower triangular matrix. Instead of assigning

265   prior distributions on $\mathbf{\Sigma}$ directly, priors were assigned on $\mathbf{\sigma}$ and $\mathbf{L}$ to avoid a strong

266   dependence between $\mathbf{\sigma}$ and $\mathbf{\Omega}$ (Lewandowski *et al.*, 2009; Alvarez *et al.*, 2016). A prior for $\mathbf{L}$

267   was specified as a so-called LKJ distribution with shape parameter 1 (Lewandowski *et al.*,

268   2009), which is identical to a uniform distribution on the space of correlation matrices. Priors

269   for $\mathbf{\sigma}$ were specified as uniform distributions with range (0, 10,000). Priors for α, β_1, β_2, r_p

270   and r_s in Eqs. 4-6, 8-10, and 13-14 were specified as normal distributions with mean 0 and

271   variance 10,000. Priors for f_i in Eqs. (2, 3, 8-10, 14), and θ_L in Eqs. (13-14) were specified as

272   uniform distributions with range (0, 1).

273   Alternative priors for f_i were considered, but none were presented as main results,

274   because the alternative priors produced statistical artifacts (Notes S4). In order to constrain

275   the latent variables in our model, a natural choice is to implement hyper-parameters to

276   describe prior means of the latent variables (e.g., different prior means of f_i for deciduous vs

277   evergreen leaves). However, analyses of simulated data suggest that using hyper-parameters

278   in our model results in biased inference for f_i as well as regression parameters (Notes S4).

279   Models were fit using the Hamiltonian Monte Carlo algorithm (HMC) implemented

280   in Stan (Carpenter *et al.*, 2016). Posterior estimates were obtained from three independent

281   chains of 20,000 iterations after a burn-in of 10,000 iterations, thinning at intervals of 20. The

282   Stan code use to fit models are available from Github at:

283   https://github.com/mattocci27/LMApLMAs. Convergence of the posterior distribution was

284   assessed with the Gelman-Rubin statistic with a convergence threshold of 1.1 for all

285   diagnostics (Gelman *et al.*, 2014a).

286

287   **Model selection**

288   Alternative LL models (Eqs. 5 and 13; see also Notes S3) fit to Panama data were compared

289   using the WAIC (Watanabe-Akaike information criterion) (Watanabe, 2010; Gelman *et al.*,

290   2014b). WAIC is a predictive information criterion for Bayesian models, with lower values

291   indicating a more parsimonious model (Gelman *et al.*, 2014b). Compared to AIC (Akaike,

292   1973) and DIC (Spiegelhalter *et al.*, 2002), WAIC has the desirable property of averaging

9

293   over the posterior distribution rather than conditioning on a point estimate (Gelman *et al.*,

294   2014b).

295

296   **Variance partitioning**

297   We used the following identity to estimate the relative contributions of LMAp and LMAs to

298   LMA variance, where again LMA = LMAp + LMAs:

299    $Var\,(Y = X1 + X1) = Cov(Y, X1 + X2) = Cov(Y, X1) + Cov(Y, X2)$ (15)

300   Thus, the fractions of total LMA variance due to variance in LMAp and LMAs were

301   determined by the covariances Cov(LMA, LMAp) and Cov(LMA, LMAs), respectively,

302   taken as proportions of the total variance Var(LMA). Tests with simulated data confirm that

303   our modeling approach can effectively partition LMA variance into LMAp and LMAs

304   components (Notes S4).

305

306   **Randomized LMA datasets**

307   Because our statistical approach includes one latent variable f_i to partition LMA into LMAp

308   and LMAs for each leaf sample, one might expect a good match between predictions and

309   observations simply due to the large number of free parameters, whether or not the model

310   captured important biological mechanisms. To evaluate model performance while controlling

311   for the number of free parameters, we compared the fit of our model to observed and

312   randomized datasets. Specifically, we generated randomized datasets by randomizing LMA

313   values across species, while maintaining the original (non-randomized) data for A_{area}, R_{area}

314   and LL. Thus, the randomized LMA datasets had zero expected covariance between LMA

315   and other traits, but maintained the observed covariances among A_{area}, R_{area} and LL. If the fit

316   between model and data depended primarily on the number of parameters or other model

317   assumptions, then we would expect similar fits for the original (non-randomized) and

318   randomized LMA datasets. For the Panama dataset, which includes two sites (wet and dry)

319   and two canopy strata (sun and shade), we also considered constrained randomizations in

320   which LMA was randomized across canopy strata within each site. We generated 10

321   randomized datasets for each analysis. Analyzing a larger number of randomized datasets

322   (e.g., 1000) was impractical given our computationally intensive Bayesian modeling

323   approach.

324   To compare model results obtained from the observed (non-randomized) dataset to

325   those obtained from the randomized datasets, we calculated the standardized effect size (SES)

326   for correlations of interest (e.g., between LMAp and A_{area}, or between LMAs and LL) as SES

327    $= (r_{obs} - r_{rand})/SD_{rand}$, where r_{obs} is the Pearson correlation coefficient of interest for the

328   observed dataset, and r_{rand} and SD_{rand} are the mean and standard deviation, respectively, of the

329   corresponding correlation coefficients for the randomized datasets. Under the null hypothesis

330   of equal correlations for the observed and randomized data, the distribution of SES is

331   approximately standard normal (Gotelli & Rohde, 2002), which we assumed when

332   calculating P-values. A significant difference ($P < 0.05$) indicates that the correlation inferred

333   from the observed dataset is different from what would be expected to emerge from model

334   assumptions and free parameters.

335

336   **Results**

337   **1. Photosynthetic and structural LMA components (LMAp and LMAs, respectively)**

338   **can be accurately estimated.**

339   Tests with simulated data show that our modeling approach can accurately partition LMA

340   into LMAp and LMAs, except in cases where the assumed relationships (e.g., between

341   LMAp and A_{area}, and between LMAs and LL) are weak (Notes S4). However, tests with

342   simulated data also show that the LMA-randomization test we implemented can effectively

343   diagnose these weak-correlation cases (Notes S4). Therefore, in all cases presented below

344   where results based on observed data are significantly different ($P < 0.05$) than results based

345   on randomized data, we assume that estimates of LMAp and LMAs (Eqs. 1-3) are accurate

346   and that the results reflect meaningful patterns in the data.

347

348   **2. Nearly all leaf dark respiration is associated with photosynthetic leaf mass.**

349   Photosynthetic mass (LMAp) accounted for nearly all leaf dark respiration; i.e., estimated

350   dark respiration rate per-unit structural mass (r_s) was close to zero in analyses of both

351   GLOPNET and Panama data (Table S1). Thus, although building costs are likely similar for

352   different leaf chemical components and tissues (Williams *et al.*, 1989; Villar & Merino,

353   2001), our results suggest that leaf mass associated with photosynthetic function accounts for

354   nearly all leaf maintenance respiration.

355

356   **3. Decomposing LMA into photosynthetic and structural components leads to improved**

357   **predictions of A_{area}, R_{area} and LL.**

358   For the GLOPNET global dataset, A_{area} had a strong positive correlation with LMAp, a weak

359   negative correlation with LMAs, and a non-significant correlation with total LMA (Figs. 1a-

360   c; Table S2). A_{area} was also positively correlated with LMAp in the randomized datasets (in

11

361 which LMA was randomized among leaves in GLOPNET; see gray symbols in Fig. 1), but

362 these correlations were weaker than those obtained from the observed data ($P < 0.001$ for the

363 null hypothesis of equal correlation in observed and randomized datasets). R_{area} in GLOPNET

364 also had a strong positive correlation with LMAp, which was stronger than the correlation

365 between R_{area} and LMAp in the randomized datasets ($P < 0.001$), or between R_{area} and either

366 LMA or LMAs (Figs. 1d-f). Finally, LL in GLOPNET had a strong positive correlation with

367 LMAs, which was stronger than the correlation between LL and LMAs from the randomized

368 datasets ($P < 0.001$) or between LL and either LMA or LMAp (Figs. 1g-i).

369   For the Panama dataset, we evaluated multiple models due to the availability of both

370 sun and shade leaves. The Optimal LL Model (Eq. 13) fit the data better than the Potential LL

371 Model (Eq. 5) according to the Watanabe-Akaike information criterion (WAIC; Table S1).

372 Including site effects in the Optimal LL Model further improved the WAIC but led to similar

373 parameter estimates and inferences (Table S1-3). All Panama results we report are for the

374 Optimal LL Model with site effects unless stated otherwise. A_{area} and R_{area} had stronger and

375 more positive correlations with LMAp than with LMA or LMAs (Figs. 2a-f and Table S3).

376 LL was not significantly correlated with LMA when all leaves were combined, but was

377 strongly correlated with LMA for shade leaves at the dry site (Fig. 2g). The correlation

378 between LL and LMAp was similar for observed and randomized datasets (Fig. 2h; Table

379 S3), implying a lack of meaningful correlation between LL and LMAp in the Panama data.

380 The correlation between LL and LMAs was weaker in observed than in randomized data

381 (Fig. 2i) because the LL vs. LMAs relationship ignores important factors in the Optimal LL

382 Model (e.g., effects of light on realized photosynthetic rates and thus optimal LL). The

383 correlation between predicted and observed LL was higher in the Optimal LL Model ($r =$

384 0.81) than for randomized datasets ($P < 0.001$), and also stronger than for the Potential LL

385 Model ($r = 0.38$) (Fig. 3; Table S4).

386

387 **4. Most interspecific LMA variation is due to variation in structural leaf mass, not**

388 **photosynthetic leaf mass.**

389 LMAs accounted for the majority of interspecific variation in LMA among all leaves in

390 GLOPNET (74.7%), among sun leaves in Panama (57.8%), and among shade leaves in

391 Panama (86.0%) (Fig. 4).

392

393 **5. Evergreen leaves have greater LMAs than deciduous leaves, and sun leaves have both**

394 **greater LMAp and LMAs than shade leaves.**

12

395   In the GLOPNET dataset, evergreen leaves had significantly higher LMAs than deciduous

396   leaves, but the two groups had similar LMAp (Fig. 5). Thus, the higher total LMA in

397   evergreen leaves in GLOPNET was primarily due to differences in LMAs (which comprised

398   a greater fraction of LMA in evergreen than in deciduous leaves; Fig. S1a). Similar results

399   were obtained for the Panama dataset (evergreen leaves have higher LMAs but similar LMAp

400   compared to deciduous leaves; Fig. S1b). In the Panama dataset, both LMAp and LMAs were

401   significantly higher in sun leaves than in shade leaves (Fig. 5). Thus, in contrast to

402   interspecific variation in LMA (which is primarily driven by variation in LMAs; Fig. 4),

403   intraspecific variation in LMA reflects changes in both LMAs and LMAp.

404

405   **6. Nitrogen and phosphorus per-unit leaf area are strongly correlated with LMAp, and**

406   **cellulose per-unit leaf area is strongly correlated with LMAs.** In the GLOPNET dataset,

407   N_{area} and P_{area} had strong positive correlations with LMAp, but only weak correlations with

408   LMAs (Fig. S3). Similarly, in the Panama dataset, N_{area} and P_{area} had strong positive

409   correlations with LMAp, but were not correlated with LMAs (Fig. 6). In contrast, cellulose

410   per-unit leaf area (CL_{area}), which was available for the Panama dataset but not for GLOPNET,

411   had a strong positive correlation with LMAs, and a weak positive correlation with LMAp

412   (Fig. 6). CL_{area} was more strongly correlated with LMA than with LMAp or LMAs, but sun

413   and shade leaves aligned along a common CL_{area}-LMAs relationship, as opposed to being

414   offset for LMA and LMAp (Figs. 6g-i). The above correlations (N_{area} and P_{area} with LMAp,

415   and CL_{area} with LMAs) were stronger than those based on randomized datasets ($P < 0.001$ in

416   all cases, Fig. 6 and Fig. S3).

417

418   **Discussion**

419   Our analyses demonstrate that decomposing LMA variation into separate photosynthetic and

420   structural components (LMAp and LMAs, respectively) leads to improved predictions of

421   photosynthetic capacity (A_{max}), dark respiration rate (R_{dark}), and leaf lifespan (LL), as well as

422   clear relationships with traits used for independent model evaluation (nitrogen, phosphorus,

423   and cellulose concentrations). Tests with simulated data suggest that our results are robust

424   and reflect meaningful, previously unreported patterns in leaf trait data. Below, we elaborate

425   on the insights gained from our analysis and the implications of our results for the

426   representation of leaf functional diversity in global ecosystem models.

427   Decomposing LMA into LMAp and LMAs provides insights into why interspecific

428   variation in leaf traits related to photosynthesis and metabolism are primarily area-dependent

13

429   (i.e., primarily independent of LMA when expressed per-unit area) rather than mass-

430   dependent (see Notes S1-2 and Osnas *et al.* 2013 for explanation of trait mass- vs. area-

431   dependence). Specifically, our results suggest that most interspecific LMA variation across

432   the global flora and across tropical tree species in Panama is due to variation in leaf mass

433   components that contribute to LL but not to A_{max} (Fig. 4). An illustrative case is the

434   comparison of evergreen and deciduous leaves in the global flora: according to our model

435   results, evergreen leaves have greater LMAs (and thus greater LL) but similar LMAp (and

436   thus similar A_{area}) compared to deciduous leaves (Figs. 1 and 5). This comparison illustrates

437   why interspecific LMA variation is largely unrelated to area-based A_{max}, which in turn

438   explains trait area-dependence (Notes S1-2). Consistent with this explanation, the assemblage

439   we examined where LMAs accounted for the highest fraction of total LMA variation (86%

440   for Panama shade leaves; Fig. 4) is also the assemblage with the highest degree of trait area-

441   dependence (Osnas *et al.* in review).

442   Decomposing LMA also provides insights as to why intraspecific patterns of trait

443   variation differ from those observed across species. In contrast to interspecific LMA

444   variation, our analysis suggests that LMAp contributes half or more of the intraspecific

445   increase in LMA from shade to sun (Figs. 5 and S1). The increase in LMAp from shade to

446   sun – which likely reflects an increase in the size and number of palisade mesophyll cells

447   with increasing light availability (Onoda *et al.*, 2008; Terashima *et al.*, 2011) – is also

448   associated with an increase in LMAs from shade to sun (Fig. 5). This positive covariance

449   between LMAp and LMAs within species means that per-area values of LMAp-dependent

450   traits (e.g., A_{area}) have a strong, positive relationship with total LMA, which implies trait

451   mass-dependence (Notes S1-2). In contrast, because interspecific variation in LMA is due

452   primarily to variation in LMAs rather than LMAp, LMAp-dependent traits (when expressed

453   per-unit area) are largely independent of LMA across species, which implies trait area-

454   dependence (Notes S1-2).

455   Finally, decomposing LMA provides insights into the intraspecific LL 'counter-

456   gradient' (Osada *et al.* 2001; Lusk *et al.* 2008; Russo & Kitajima 2016), whereby LL

457   decreases as LMA increases from shade to sun within species, which contrasts with positive

458   interspecific LL-LMA relationships within a single light environment. Decomposing LMA

459   into LMAp and LMAs suggests that the decline in photosynthetic rate from sun to shade

460   (which increases optimal LL from a carbon-gain perspective; Kikuzawa 1991) is sufficient to

461   produce an intraspecific counter-gradient, because a counter-gradient occurs at the dry

462   Panama site (6 vs. 8 months for sun vs. shade LL means) despite no change in the structural

14

463   leaf mass fraction (LMAs/LMA) from sun to shade (see LMAp/LMA values in Fig. S1c, with

464   LMAs/LMA = 1 – LMAp/LMA). However, the counter-gradient is stronger at the wet

465   Panama site (11 vs. 31 months for sun vs. shade LL means), where LMAs/LMA is

466   significantly higher for shade leaves than for sun leaves (see LMAp/LMA in Fig. S1c). Thus,

467   at the wet Panama site, changes in LMAs/LMA from sun to shade appear to strengthen the

468   counter-gradient. The potential for LMAs/LMA to enhance the counter-gradient is

469   corroborated by data on cellulose percent mass, which is similar in shade and sun at the

470   Panama dry site (Fig. S4b; as observed by Lusk *et al.* 2010), but higher in shade than sun at

471   the wet site (Fig. S4b; as observed by Kitajima *et al.*, 2016). In summary, the decrease in

472   optimal LL with increasing light (Kikuzawa 1991) appears sufficient by itself to create a LL

473   counter-gradient, but the counter-gradient appears to be enhanced in some assemblages by

474   greater structural mass fractions in shade vs. sun leaves.

475   The improved predictions and understanding provided by decomposing LMA into

476   photosynthetic and structural components challenge the view that leaf functional diversity

477   can be accurately represented by a single leaf economics spectrum (LES) axis (Wright *et al.*

478   2004). Lloyd *et al.* (2013) argued that the apparent dominance of a single LES axis is an

479   artifact of expressing area-dependent leaf traits on a per-mass basis, and Osnas *et al.* (2013)

480   demonstrated that across the global flora, traits related to photosynthesis and metabolism are

481   indeed area-dependent. Intraspecific patterns in trait variation, which contrast with

482   interspecific patterns, pose additional challenges for a one-dimensional view of leaf

483   functional diversity. Our analysis shows that considering two primary axes of leaf trait

484   variation (photosynthesis and structure) provides improved quantitative predictions and

485   insights compared to a single LES. Our results point to a simple two-dimensional framework

486   for representing leaf functional diversity in global ecosystem models: a LMAp axis that

487   determines $A_{\max}$, accounts for nearly all R_{dark} (see r_p and r_s estimates in Table S1), and affects

488   LL as predicted by optimality theory (Kikuzawa 1992); and a LMAs axis that determines

489   potential LL through its effects on leaf toughness (Kitajima *et al.* 2012). In the datasets we

490   analyzed (the global flora and tropical trees in Panama), these two axes are only weakly

491   correlated with each other (Fig. S5), which suggests that trait-based approaches to global

492   ecosystem modeling (Scheiter *et al.*, 2013; Wullschleger *et al.*, 2014) could consider these as

493   independent axes.

494   Our statistical decomposition of LMA into photosynthetic and structural components

495   provides important insights (summarized above), but additional insights and accuracy could

496   be gained by a more mechanistic modeling approach. For example, John *et al.* (2017)

497   decomposed interspecific LMA variation into anatomical components such as the size,

498   number of layers, and mass density of cells in different leaf tissues. If such detailed

499   information became available for a large number of leaves, representing both intra- and

500   interspecific variation, it should be possible to quantify how these anatomical traits scale up

501   to leaf-level A_{max} , R_{dark}, and LL. A simpler alternative would be to modify our model (see

502   methods) to account for variation in cell wall thickness (T_{CW}): for a given cell size, increasing

503   T_{CW} would lead to an increase in lamina density, cellulose per volume, toughness, and LL

504   (Kitajima and Poorter 2010; Kitajima *et al.* 2012, 2016), and a decrease in mesophyll

505   conductance and A_{max} (Evans *et al.*, 2009; Terashima *et al.*, 2011; Onoda *et al.*, 2017).

506

507   **Conclusions**

508   It is widely recognized that LMA variation is associated with multiple tissues and functions,

509   including metabolically active mesophyll that largely determines photosynthetic capacity, as

510   well as structural and chemical components that contribute primarily to leaf toughness and

511   defense (Roderick *et al.*, 1999; Shipley *et al.*, 2006; Lusk *et al.*, 2010). It should not be

512   surprising then, that partitioning LMA into photosynthetic and structural components yields

513   enhanced predictions and improved understanding of patterns of leaf trait variation both

514   within and among species. Yet for over a decade, the vast literature on leaf traits has been

515   strongly influenced by the view that leaf trait variation can usefully be represented by a single

516   LES axis. Our results provide quantitative evidence that this one-dimensional view of leaf

517   trait variation is insufficient, and our model provides a biological explanation for previous

518   statistical analyses that have demonstrated area-dependence of leaf traits across species

519   (Osnas *et al.* 2013), while also explaining mass-dependence within species. Our results

520   suggest that most of the interspecific variation in LMA concerns structural mass that

521   contributes to LL but not to photosynthetic capacity, and that structural and photosynthetic

522   LMA components are only weakly correlated across species. Thus, strong interspecific

523   correlations between LMA and mass-normalized photosynthetic capacity (and related traits,

524   such as respiration rate, and nitrogen and phosphorus concentrations) are likely driven by

525   mass-normalization itself, rather than any functional dependence of these photosynthetic and

526   metabolic traits on LMA (Lloyd *et al.* 2013, Osnas *et al.* 2013). In contrast, intraspecific

527   variation in LMA is driven by coordinated changes in structural and photosynthetic mass

528   components, which explains why mass-normalized photosynthetic and metabolic traits vary

529   little from sun to shade within species (Aranda *et al.*, 2004; Poorter *et al.*, 2006; Niinemets *et*

530   *al.*, 2014).

531

Acknowledgments

We thank Jonathan Dushoff for statistical advice and Martijn Slot for helpful comments that improved the paper. Mirna Samaniego and Milton Garica provided indispensable assistance in data collection. We thank the Smithsonian Tropical Research Institute (STRI), the Tropical Canopy Biology Program at STRI and the Andrew W. Mellon Foundation for supporting this work. MK was supported by a Postdoctoral Fellowship for Research Abroad from the Japan Society for the Promotion of Science.

Author contributions:

MK, JWL and JLDO conceived of the study; KK, SJW and SAVB contributed data; MK devised the analytical approach and performed analyses; MK and JWL wrote the first draft of the manuscript, and all authors contributed to revisions.

References

Akaike H. **1973**. Information theory and an extension of the maximum likelihood principle.Petrov BN, Csaki F eds. Akadémiai Kiado, 267–281.

Alvarez I, Niemi J, Simpson M. **2016**. Bayesian Inference for a Covariance Matrix. *arXiv preprint arXiv:1408.4050v2*: 1–12.

Aranda I, Pardo F, Gil L, Pardos JA. **2004**. Anatomical basis of the change in leaf mass per area and nitrogen investment with relative irradiance within the canopy of eight temperate tree species. *Acta Oecologica* **25**: 187–195.

Bishop CM. **2006**. Pattern Recognition and Machine Learning.

Bonan GB, Levis S, Kergoat L, Oleson KW. **2002**. Landscapes as patches of plant functional types: An integrating concept for climate and ecosystem models. *Global Biogeochemical Cycles* **16**: 5–1–5–23.

Carpenter B, Gelman A, Hoffman M, Lee D, Goodrich B. **2016**. Stan: A probabilistic programming language. *J Stat Softw*.

Ellsworth DS, Reich PB. **1993**. Canopy structure and vertical patterns of photosynthesis and related leaf traits in a deciduous forest. *Oecologia*.

Evans JR, Kaldenhoff R, Genty B, Terashima I. **2009**. Resistances along the CO2 diffusion pathway inside leaves. *Journal of Experimental Botany* **60**: 2235–2248.

Gelman A, Hill J. **2006**. Data analysis using regression and multilevel/hierarchical models.

Gelman A, Carlin JB, Stern HS, Dunson DB, Vehtari A, Rubin DB. **2014a**. *Bayesian*

565   *Data Analysis, Third Edition*. Taylor & Francis.

566 **Gelman A, Hwang J, Vehtari A**. **2014b**. Understanding predictive information criteria for

567   Bayesian models. *Statistics and Computing* **24**: 997–1016.

568 **Gotelli N, Rohde K**. **2002**. Co-occurrence of ectoparasites of marine fishes: a null model

569   analysis. *Ecology Letters* **5**: 86–94.

570 **John GP, Scoffoni C, Buckley TN, Villar R, Poorter H, Sack L**. **2017**. The anatomical and

571   compositional basis of leaf mass per area. *Ecology Letters*.

572 **Kenzo T, Ichie T, Watanabe Y, Yoneda R, Ninomiya I, Koike T**. **2006**. Changes in

573   photosynthesis and leaf characteristics with tree height in five dipterocarp species in a

574   tropical rain forest. *Tree Physiology* **26**: 865–873.

575 **Kikuzawa K**. **1991**. A cost-benefit analysis of leaf habit and leaf longevity of trees and their

576   geographical pattern. *The American Naturalist*: 1250–1263.

577 **Kikuzawa K, Onoda Y, Wright IJ, Reich PB**. **2013**. Mechanisms underlying global

578   temperature-related patterns in leaf longevity. *Global Ecology and Biogeography*.

579 **Kikuzawa K, Shirakawa H, Suzuki M, Umeki K**. **2004**. Mean labor time of a leaf.

580   *Ecological Research* **19**: 365–374.

581 **Kitajima K, Llorens A-M, Stefanescu C, Timchenko MV, Lucas PW, Wright SJ**. **2012**.

582   How cellulose-based leaf toughness and lamina density contribute to long leaf

583   lifespans of shade-tolerant species. *New Phytologist* **195**: 640–652.

584 **Kitajima K, Wright SJ, Westbrook JW**. **2016**. Leaf cellulose density as the key

585   determinant of inter- and intra-specific variation in leaf fracture toughness in a

586   species-rich tropical forest. *Interface Focus* **6**: 20150100–9.

587 **Lewandowski D, Kurowicka D, Joe H**. **2009**. Generating random correlation matrices based

588   on vines and extended onion method. *Journal of Multivariate Analysis* **100**: 1989–

589   2001.

590 **Lloyd J, Bloomfield K, Domingues TF, Farquhar GD**. **2013**. Photosynthetically relevant

591   foliar traits correlating better on a mass vs an area basis: of ecophysiological

592   relevance or just a case of mathematical imperatives and statistical quicksand? *New*

593   *Phytologist* **199**: 311–321.

594 **Lusk C, Onoda Y, Kooyman R, Gutiérrez-Girón A**. **2010**. Reconciling species-level vs

595   plastic responses of evergreen leaf structure to light gradients: shade leaves punch

596   above their weight. *New Phytologist* **186**: 429–438.

597 **Lusk CH, Reich PB, Montgomery RA, Ackerly DD, Cavender-Bares J**. **2008**. Why are

598   evergreen leaves so contrary about shade? *Trends in Ecology & Evolution* **23**: 299–
599   303.

600 **Niinemets Ü, Keenan TF, Hallik L**. **2014**. A worldwide analysis of within-canopy
601   variations in leaf structural, chemical and physiological traits across plant functional
602   types. *New Phytologist* **205**: 973–993.

603 **Onoda Y, Schieving F, Anten NPR**. **2008**. Effects of light and nutrient availability on leaf
604   mechanical properties of Plantago major: a conceptual approach. *Annals of botany*
605   **101**: 727–736.

606 **Onoda Y, Wright IJ, Evans JR, Hikosaka K, Kitajima K, Niinemets Ü, Poorter H,**
607   **Tosens T, Westoby M**. **2017**. Physiological and structural tradeoffs underlying the
608   leaf economics spectrum. *New Phytologist*.

609 **Osada N, Takeda H, Furukawa A, Awang M**. **2001**. Leaf dynamics and maintenance of
610   tree crowns in a Malaysian rain forest stand. *Journal of Ecology* **89**: 774–782.

611 **Osnas JLD, Lichstein JW, Reich PB, Pacala SW**. **2013**. Global Leaf Trait Relationships:
612   Mass, Area, and the Leaf Economics Spectrum. *Science* **340**: 741–744.

613 **Poorter H, Pepin S, Rijkers T, de Jong Y, Evans JR, Körner C**. **2006**. Construction costs,
614   chemical composition and payback time of high- and low-irradiance leaves. *Journal*
615   *of Experimental Botany* **57**: 355–371.

616 **Reich PB**. **2014**. The world-wide 'fast-slow' plant economics spectrum: a traits manifesto (H
617   Cornelissen, Ed.). *Journal of Ecology* **102**: 275–301.

618 **Reich PB, Walters MB, Ellsworth DS**. **1997**. From tropics to tundra: global convergence in
619   plant functioning. *Proceedings of the National Academy of Sciences* **94**: 13730–
620   13734.

621 **Roderick ML, Berry SL, Noble IR, Farquhar GD**. **1999**. A theoretical approach to linking
622   the composition and morphology with the function of leaves. *Functional Ecology* **13**:
623   683–695.

624 **Russo SE, Kitajima K**. **2016**. The Ecophysiology of Leaf Lifespan in Tropical Forests:
625   Adaptive and Plastic Responses to Environmental Heterogeneity.Goldstein G,
626   Santiago SL eds. Tropical Tree Physiology: Adaptations and Responses in a Changing
627   Environment. Tropical Tree Physiology. Cham: Springer International Publishing,
628   357–383.

629 **Scheiter S, Langan L, Higgins SI**. **2013**. Next-generation dynamic global vegetation
630   models: learning from community ecology. *New Phytologist* **198**: 957–969.

631 **Shipley B, Lechowicz M, Wright I, Reich P**. **2006**. Fundamental trade-offs generating the

632   worldwide leaf economics spectrum. *Ecology* **87**: 535–541.

633   **Spiegelhalter DJ, Best NG, Carlin BP, Van Der Linde A**. **2002**. Bayesian measures of

634   model complexity and fit. *Journal of the Royal Statistical Society: Series B*

635   *(Statistical Methodology)* **64**: 583–639.

636   **Terashima I, Hanba YT, Tholen D, Niinemets Ü**. **2011**. Leaf functional anatomy in

637   relation to photosynthesis. *Plant Physiology* **155**: 108–116.

638   **Villar R, Merino J**. **2001**. Comparison of leaf construction costs in woody species with

639   differing leaf life-spans in contrasting ecosystems. *New Phytologist*.

640   **Watanabe S**. **2010**. Asymptotic Equivalence of Bayes Cross Validation and Widely

641   Applicable Information Criterion in Singular Learning Theory. *The Journal of*

642   *Machine Learning Research* **11**: 3571–3594.

643   **Westoby M, Wright IJ**. **2006**. Land-plant ecology on the basis of functional traits. *Trends in*

644   *Ecology & Evolution* **21**: 261–268.

645   **Williams K, Field CB, Mooney HA**. **1989**. Relationships among leaf construction cost, leaf

646   longevity, and light environment in rain-forest plants of the genus Piper. *The*

647   *American Naturalist*.

648   **Wright IJ, Reich PB, Westoby M, Ackerly DD, Baruch Z, Bongers F, Cavender-Bares J,**

649   **Chapin T, Cornelissen J, Diemer M, *et al.* 2004**. The worldwide leaf economics

650   spectrum. *Nature* **428**: 821–827.

651   **Wright SJ, Horlyck V, Basset Y, Barrios H, Bethancourt A, Bohlman SA, Gilbert GS**.

652   **2003**. Tropical Canopy Biology Program, Republic of Panama.Basset Y, Horlyck V,

653   Wright SJ eds. Studying Forest Canopies from Above: The International Canopy

654   Crane Network. Panama, 137–155.

655   **Wullschleger SD, Epstein HE, Box EO, Euskirchen ES, Goswami S, Iversen CM, Kattge**

656   **J, Norby RJ, van Bodegom PM, Xu X**. **2014**. Plant functional types in Earth system

657   models: past experiences and future directions for application of dynamic vegetation

658   models in high-latitude ecosystems. *Annals of botany* **114**: 1–16.

659

660

661 **Supporting information**

662 **Notes S1** Defining and understanding leaf trait mass- vs. area-dependence.

663 **Notes S2** Implications of photosynthetic and structural leaf mass for trait mass- vs. area-

664 dependence.

665 **Notes S3** Alternative leaf lifespan models and realized net photosynthesis.

666 **Notes S4** Model tests with simulated data.

667 **Fig. S1** Boxplots comparing posterior means of the latent variable f (the fraction of total

668 LMA comprised by LMAp) across deciduous (D) and evergreen (E) leaves in GLOPNET and

669 Panama, and across sites (wet and dry) and canopy strata (sun and shade) in Panama.

670 **Fig. S2** Boxplots comparing leaf mass per area (LMA), photosynthetic leaf mass per area

671 (LMAp; posterior means), and structural leaf mass per area (LMAs; posterior means) across

672 sites (wet and dry) and canopy strata (sun and shade) in all leaves in the Panama datasets.

673 **Fig. S3** Measured traits related to photosynthesis and metabolism (nitrogen and phosphorus

674 per-unit leaf area; N_{area} and P_{area}) are positively correlated with LMA and with estimates

675 (posterior means) of the photosynthetic and structural LMA components (LMAp and LMAs,

676 respectively) in the GLOPNET dataset.

677 **Fig. S4** Boxplots comparing cellulose content (percent of total leaf mass) across sites (wet

678 and dry) and canopy strata (sun and shade) in Panama.

679 **Fig. S5** Posterior means of LMAp vs LMAs in the (a) GLOPNET and (b) Panama datasets.

680 **Table S1** Summary of results for Potential LL Model (Eq. 5) and Optimal LL Models (Notes

681 S3).

682 **Table S2** Correlations between LMAp or LMAs and other traits derived from the Potential

683 LL model (Eq. 5) fit to GLOPNET data.

684 **Table S3** Correlations between LMAp or LMAs and other traits derived from the three

685 alternative LL models (Notes S3) fit to Panama data.

686 **Table S4** Correlations between observed and predicted LL for the Potential LL Model (Eq. 5)

687 and the Optimal LL Model (Notes S3) fit to Panama data.

688

689   **Figure legends**

690   **Fig. 1** Observed and estimated leaf-trait relationships in the global GLOPNET dataset. Leaf

691   life span (LL), net photosynthetic rate per unit leaf area (A_{area}), and dark respiration rate per

692   unit leaf area (R_{area}) are plotted against observed LMA and estimates (posterior means) of

693   photosynthetic and structural LMA components (LMAp and LMAs, respectively). Gray

694   symbols show 1 of 10 randomized datasets, in which LMA was randomized among all leaves

695   in the GLOPNET dataset we analyzed (which includes all leaves for which LMA, A_{area}, R_{area},

696   and LL were available). Pearson correlation coefficients are for observed LMA (left column)

697   and posterior means of LMAp (middle column) and LMAs (right column). *P*-values (** *P* <

698   0.01; *** *P* < 0.001) for LMA test the null hypothesis of zero correlation, and for LMAp and

699   LMAs test the null hypothesis of equal correlation in observed and randomized datasets (see

700   'Randomized LMA Datasets' in Methods for details). In some cases, r_{obs} is near zero but

701   significantly greater than r_{rand} because r_{rand} is negative (see Table S2 for details).

702

703   **Fig. 2** Observed and estimated leaf-trait relationships in the Panama dataset. Estimates are

704   from the Optimal LL Model with site effects (Eq. 13 and Notes S3). Details as in Fig. 1,

705   except that in the randomized dataset shown here (gray symbols), LMA was randomized

706   within sites (wet and dry) across canopy strata (sun and shade). Results for other LL models

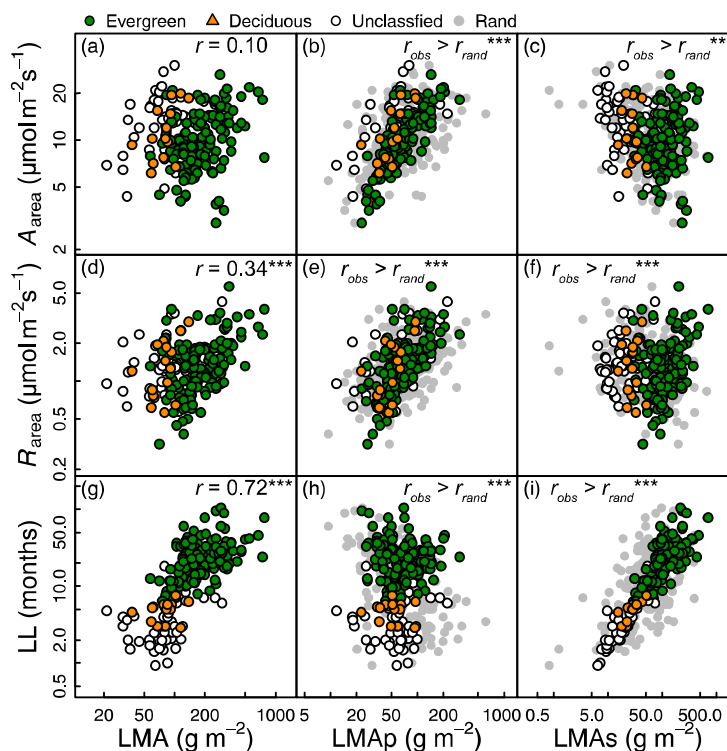707   are summarized in Table S3.

708

709   **Fig. 3** Observed vs. predicted leaf lifespan (LL) in the (a) Potential LL Model (Eq. 5) and (b)

710   Optimal LL Model with site effects (Eq. 13 and Notes S3). Predicted LL values are posterior

711   means. The dashed line indicates the 1:1 relationship. Gray symbols show predicted LL

712   values from 1 of 10 randomized LMA datasets for each model. Pearson correlation

713   coefficients are for predictions derived from the observed datasets, and *P*-values (*** *P* <

714   0.001) are for the null hypothesis of equal correlation in observed and randomized datasets

715   (see 'Randomized LMA Datasets' in Methods for details). Results for other LL models are

716   reported in Table S4.

717

718   **Fig. 4** Percent of interspecific variation in leaf mass per area (LMA) explained by

719   photosynthetic and structural components of LMA (LMAp and LMAs, respectively) for the

720   global GLOPNET dataset (GL), sun leaves in Panama (PA Sun), and shade leaves in Panama

721   (PA Shade). Variance was partitioned by applying Eq. 15 to posterior means of LMAp and

722   LMAs.

723

724   **Fig. 5** Boxplots comparing leaf mass per area (LMA) and posterior means of photosynthetic

725   and structural LMA components (LMAp and LMAs, respectively) across deciduous (D) and

726   evergreen (E) leaves in the GLOPNET dataset (top), and across sites (wet and dry) and

727   canopy strata (sun and shade) in the Panama dataset (bottom). The center line in each box

728   indicates the median, upper and lower box edges indicate the interquartile range, whiskers

729   show 1.5 times the interquartile range, and points are outliers. Groups sharing the same letters

730   are not significantly different ($P > 0.05$; t-tests). To isolate the effects of intraspecific

731   variation (i.e., plastic responses to light), the Panama results shown here only include species

732   for which both sun and shade leaves were available. Qualitatively similar results were

733   obtained when all Panama species were included (Fig. S2). Note that the vertical axis is on a

734    $\log_{10}$ scale.

735

736   **Fig. 6** Measured traits related to photosynthesis and metabolism traits (nitrogen and

737   phosphorus per-unit leaf area; N_{area} and P_{area}) are strongly correlated with estimates (posterior

738   means) of the photosynthetic LMA component (LMAp), and a measured structural trait

739   (cellulose per-unit leaf area; CL_{area}) is strongly correlated with estimates of the structural

740   LMA component (LMAs) for the Panama dataset. Note that sun and shade leaves align along

741   a single relationship for CL_{area} vs. LMAs, but not for CL_{area} vs. LMA or LMAp. N_{area}, P_{area},

742   and CL_{area} data were not used to fit the models, and are presented here as independent support

743   for the model results. Analogous results were obtained for N_{area} and P_{area} vs. LMAp for

744   GLOPNET (Fig. S3). Gray symbols show 1 of 10 datasets in which LMA was randomized

745   within sites (wet and dry) across canopy strata (sun and shade). Others details as in Fig. 1.

746   Results for other LL models are reported in Table S3.

747

748

23

749

750

Fig. 1 Observed and estimated leaf-trait relationships in the global GLOPNET dataset. Leaf life span (LL), net photosynthetic rate per unit leaf area (A_{area}), and dark respiration rate per unit leaf area (R_{area}) are plotted against observed LMA and estimates (posterior means) of photosynthetic and structural LMA components (LMAp and LMAs, respectively). Gray symbols show 1 of 10 randomized datasets, in which LMA was randomized among all leaves in the GLOPNET dataset we analyzed (which includes all leaves for which LMA, A_{area}, R_{area}, and LL were available). Pearson correlation coefficients are for observed LMA (left column) and posterior means of LMAp (middle column) and LMAs (right column). P-values (** $P <$ 0.01; *** $P <$ 0.001) for LMA test the null hypothesis of zero correlation, and for LMAp and LMAs test the null hypothesis of equal correlation in observed and randomized datasets (see 'Randomized LMA Datasets' in Methods for details). In some cases, r_{obs} is near zero but significantly greater than r_{rand} because r_{rand} is negative (see Table S2 for details).
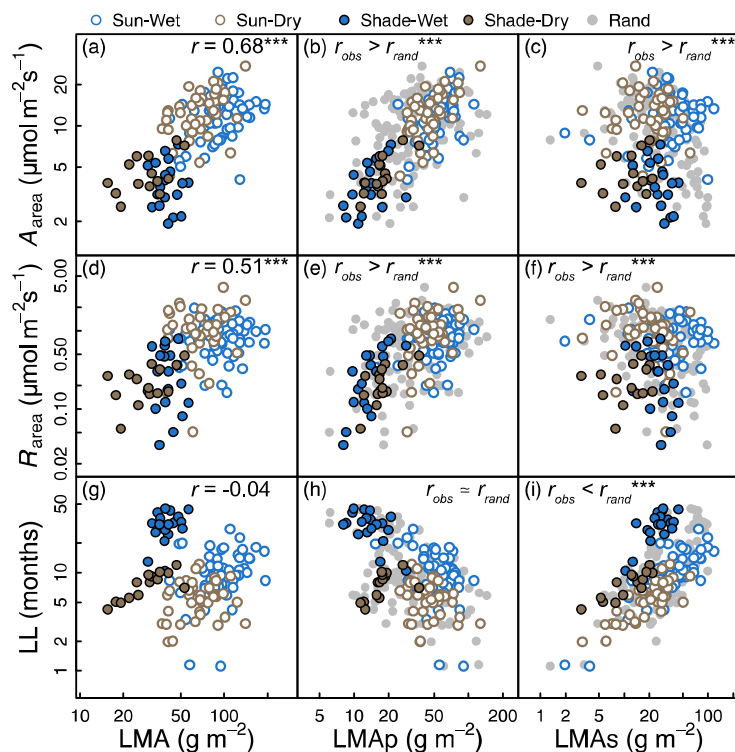
Fig. 2 Observed and estimated leaf-trait relationships in the Panama dataset. Estimates are from the Optimal LL Model with site effects (Eq. 13 and Notes S3). Details as in Fig. 1, except that in the randomized dataset shown here (gray symbols), LMA was randomized within sites (wet and dry) across canopy strata (sun and shade). Results for other LL models are summarized in Table S3.
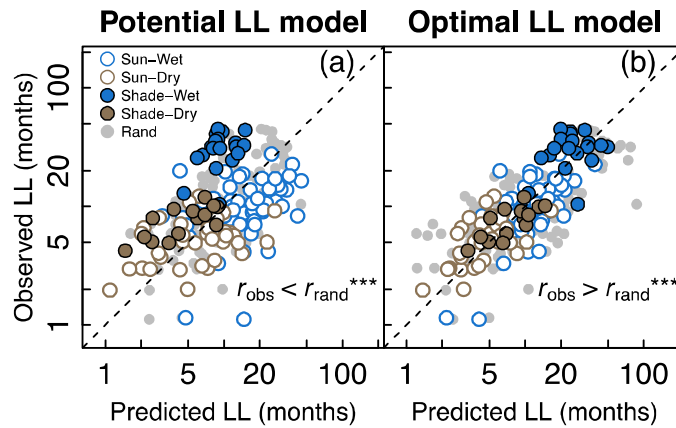
25

Fig. 3 Observed vs. predicted leaf lifespan (LL) in the (a) Potential LL Model (Eq. 5) and (b) Optimal LL Model with site effects (Eq. 13 and Notes S3). Predicted LL values are posterior means. The dashed line indicates the 1:1 relationship. Gray symbols show predicted LL values from 1 of 10 randomized LMA datasets for each model. Pearson correlation coefficients are for predictions derived from the observed datasets, and *P*-values (*** *P* < 0.001) are for the null hypothesis of equal correlation in observed and randomized datasets (see 'Randomized LMA Datasets' in Methods for details). Results for other LL models are reported in Table S4.
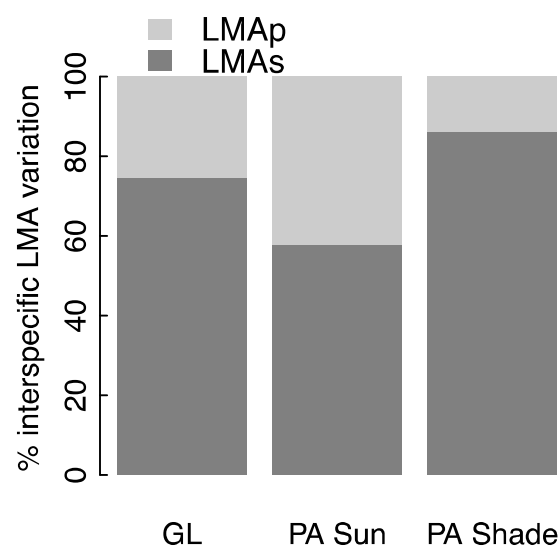
779

780   **Fig. 4** Percent of interspecific variation in leaf mass per area (LMA) explained by

781   photosynthetic and structural components of LMA (LMAp and LMAs, respectively) for the

782   global GLOPNET dataset (GL), sun leaves in Panama (PA Sun), and shade leaves in Panama

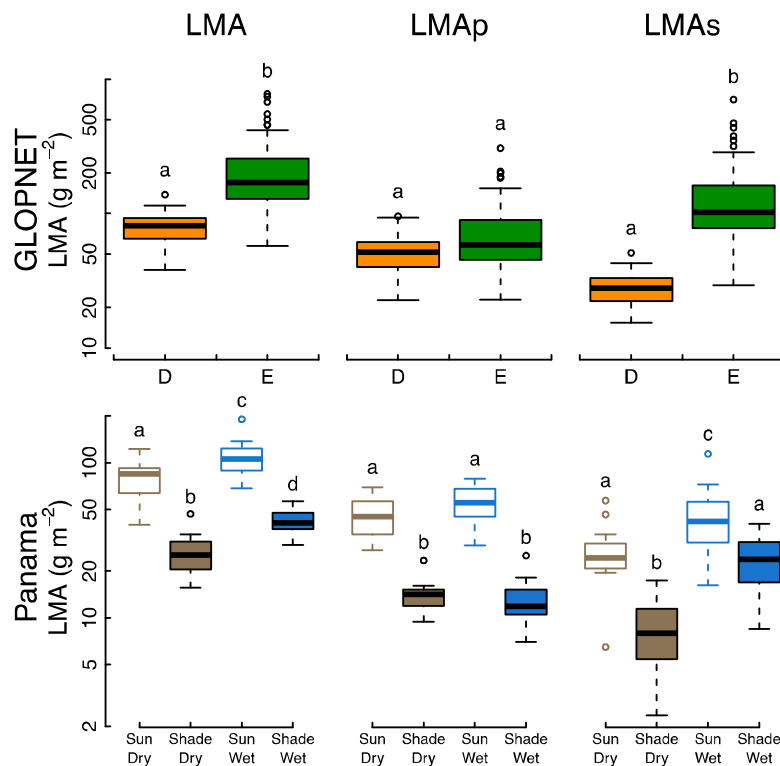783   (PA Shade). Variance was partitioned by applying Eq. 15 to posterior means of LMAp and

784   LMAs.

785

786

787

788

Fig. 5 Boxplots comparing leaf mass per area (LMA) and posterior means of photosynthetic and structural LMA components (LMAp and LMAs, respectively) across deciduous (D) and evergreen (E) leaves in the GLOPNET dataset (top), and across sites (wet and dry) and canopy strata (sun and shade) in the Panama dataset (bottom). The center line in each box indicates the median, upper and lower box edges indicate the interquartile range, whiskers show 1.5 times the interquartile range, and points are outliers. Groups sharing the same letters are not significantly different ($P > 0.05$; t-tests). To isolate the effects of intraspecific variation (i.e., plastic responses to light), the Panama results shown here only include species for which both sun and shade leaves were available. Qualitatively similar results were obtained when all Panama species were included (Fig. S2). Note that the vertical axis is on a $\log_{10}$ scale.
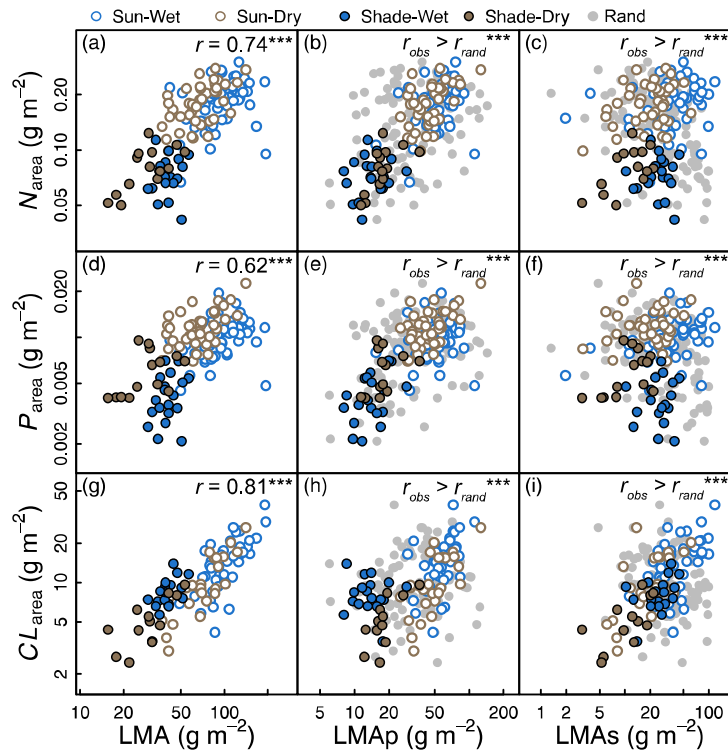
Fig. 6 Measured traits related to photosynthesis and metabolism traits (nitrogen and phosphorus per-unit leaf area; N_{area} and P_{area}) are strongly correlated with estimates (posterior means) of the photosynthetic LMA component (LMAp), and a measured structural trait (cellulose per-unit leaf area; CL_{area}) is strongly correlated with estimates of the structural LMA component (LMAs) for the Panama dataset. Note that sun and shade leaves align along a single relationship for CL_{area} vs. LMAs, but not for CL_{area} vs. LMA or LMAp. N_{area}, P_{area}, and CL_{area} data were not used to fit the models, and are presented here as independent support for the model results. Analogous results were obtained for N_{area} and P_{area} vs. LMAp for GLOPNET (Fig. S3). Gray symbols show 1 of 10 datasets in which LMA was randomized within sites (wet and dry) across canopy strata (sun and shade). Others details as in Fig. 1. Results for other LL models are reported in Table S3.